On the force balance around dipolarization fronts within bursty bulk flows

S.-S. Li,[1] V. Angelopoulos,[1] A. Runov,[1] X.-Z. Zhou,[1] J. McFadden,[2] D. Larson,[2] J. Bonnell,[2] and U. Auster[3]

Received 1 July 2010; revised 19 February 2011; accepted 25 February 2011; published 14 May 2011.

[1] We study the force balance surrounding the arrival of dipolarization fronts within bursty bulk flows near substorm onset by comparing curvature force densities and total pressure gradient force densities ahead of and behind the fronts using three inner Time History of Events and Macroscale Interactions during Substorms (THEMIS) probes separated along the Xgsm and the Zgsm directions. Curvature force density estimates are obtained by field line modeling utilizing the *Z* separation of the probes and the self-similar structure of the front over short distances. A dipolarization front is a boundary between the energetic particle population in the flow burst magnetic flux bundle and the ambient colder plasma ahead of the front. Force density imbalance is found ahead of and behind the front. Ahead of the front, decrease in tailward pressure gradient force results in earthward flow acceleration. Behind the dipolarization front, even though the radius of field line curvature increases, the curvature force density increases even further, mostly due to the increase in the magnetic field magnitude. Thus, plasma acceleration at and immediately after the dipolarization front can be explained by the resultant increased curvature force density.

Citation: Li, S.-S., V. Angelopoulos, A. Runov, X.-Z. Zhou, J. McFadden, D. Larson, J. Bonnell, and U. Auster (2011), On the force balance around dipolarization fronts within bursty bulk flows, *J. Geophys. Res.*, *116*, A00I35, doi:10.1029/2010JA015884.

1. Introduction

[2] Bursty bulk flows (BBFs), which are frequently observed in the plasma sheet, are the most efficient means of transporting energy and magnetic flux in the magnetotail [*Angelopoulos et al.*, 1994]. BBFs are often accompanied by a rapid increase in the magnetic field component normal to the undisturbed cross-tail current sheet (B_z) and a decrease in the plasma thermal pressure. These signatures are similar in the midtail and the near-Earth plasma sheet [*Ohtani et al.*, 2004]. BBF braking in the near-Earth plasma sheet at geocentric distances ~10 R_E is one of the most important elements of a magnetospheric substorm [*Shiokawa et al.*, 1998; *Baumjohann et al.*, 1999]. Questions remain, however, about how BBFs are decelerated and which factors control the depth of BBF penetration into the near-Earth plasma sheet.

[3] Impulsive magnetic reconnection in the midtail plasma sheet is generally considered to be the mechanism that generates fast flow bursts [*Sergeev et al.*, 2004]. This mechanism implies plasma acceleration and imbalance between the curvature-dependent components of the $\mathbf{j} \times \mathbf{B}$ force and the plasma pressure gradient. Recent particle-in-cell simulations of impulsive reconnection with open boundary conditions have indicated that the force balance is restored in approximately one ion gyroperiod [*Sitnov et al.*, 2009]. Individual flow bursts within BBFs, on the other hand, occasionally show "plasma bubble" properties [*Sergeev et al.*, 1996]. These bubbles are narrow, transient, earthward moving plasma streams with lower density than the ambient plasma sheet population. According to plasma bubble theory (see *Wolf et al.* [2009] for a review), the relative motion of the bubble is due to lower flux tube entropy $S = pV^{\gamma}$, where S is the entropy, and V is the flux tube volume within the bubble. The inward motion of the bubble continues until the bubble entropy (S_b) equals the entropy of the surrounding plasma. Because the parameter S is global, it is difficult (perhaps impossible) to estimate it using local spacecraft observations. Using local parameters, changes in flux tube entropy in the vicinity of the neutral sheet ($B_x \sim 0$) may be roughly estimated as $\delta S \sim \delta(p/B_z)$ [*Sergeev et al.*, 2004]. *Dubyagin et al.* [2010] conducted a detailed analysis of flux tube entropy changes in the flow-braking region using the *Wolf et al.* [2006] formula. Here we study the problem of BBF penetration into the magnetic, dipole-dominated, near-Earth plasma sheet by examining the force densities acting on the flux tube near the magnetic equator.

[4] In the ideal magnetohydrodynamic (MHD) approximation $d/dt(\mathbf{B}/\rho) = (\mathbf{B}/\rho \cdot \nabla)\mathbf{v}$, plasma (considered as a fluid with mass density ρ) and the magnetic field move together at a velocity v. Each magnetic field line, therefore, is a flux tube with a specific plasma population. Considering force

[1]Institute of Geophysics and Planetary Physics, University of California, Los Angeles, California, USA.
[2]Space Sciences Laboratory, University of California, Berkeley, California, USA.
[3]Institut für Geophysik und Extraterrestrische Physik, Technische Universität, Braunschweiger, Germany.

0148-0227/11/2010JA015884

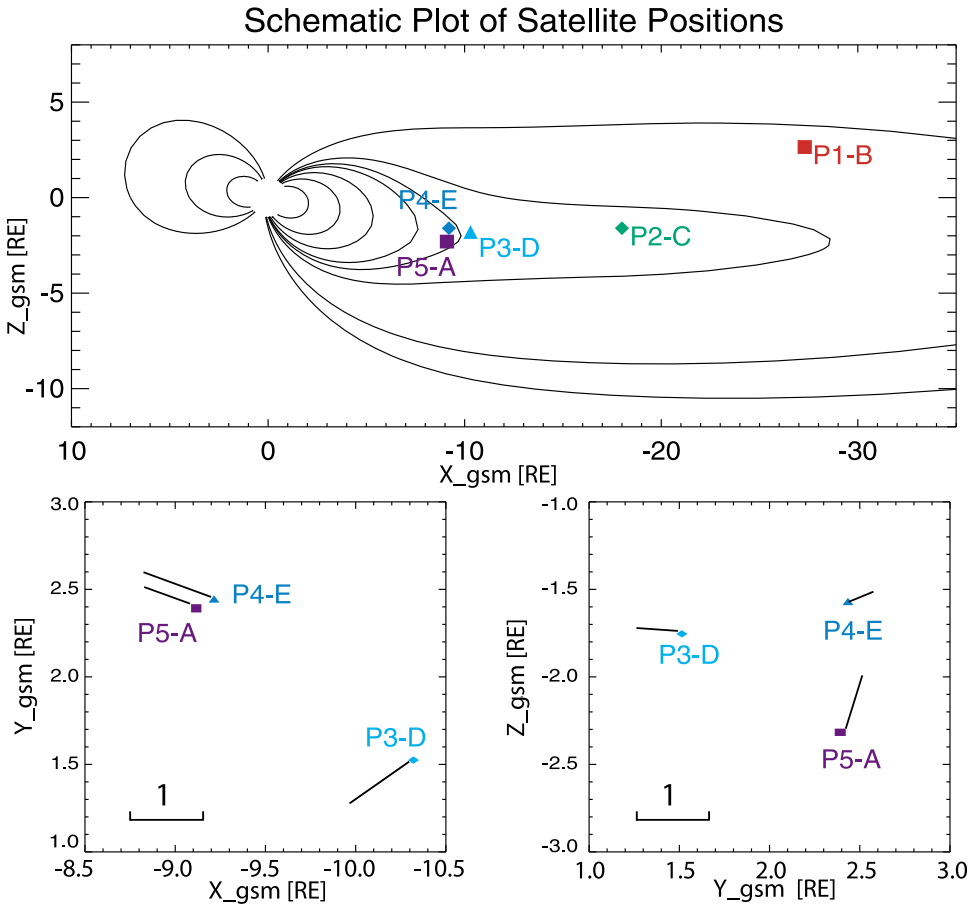

Figure 1. The three inner THEMIS probes, P3/P4/P5 (THD/THE/THA), were located close to the neutral sheet (discussed later) and separated in both the Z (P4 and P5) and X (P3 and P4) directions within a distance of about 1 R_E: P3 at (−10.3, 1.5, −1.8) R_E; P4 at (−9.2, 2.4, −1.6) R_E; P5 at (−9.1, 2.4, −2.3) R_E. The outer two probes, P1 and P2, were located at (−27.3, 13.2, 2.7) R_E and (−18.0, 1.4, −1.6) R_E. All data are shown in GSM coordinates.

densities acting on the equatorial element of a flux tube, the acceleration (or deceleration) of plasma and magnetic field in the tube is defined by the balance between the $\mathbf{j} \times \mathbf{B}$ force and the plasma thermal pressure gradient, or equivalently, between the Maxwell tension and the total pressure gradient.

[5] Ideal MHD simulations of bubble evolution in realistic 2-D geometry have shown a rapid increase in the magnetic field Z component (i.e., dipolarization front (DF) formation) during the early stages of underpopulated flux tube evolution [*Birn et al.*, 2004]. Formation of dipolarization fronts has also been shown in PIC simulations of impulsive magnetic reconnection [*Sitnov et al.*, 2009]. Recent observations by the Time History of Events and Macroscale Interactions during Substorms (THEMIS) spacecraft constellation distributed along the tail have demonstrated that dipolarization fronts may propagate from the midtail toward the near-Earth plasma sheet [*Runov et al.*, 2009]. They have also been shown to be boundaries separating hot BBF plasma from the ambient plasma sheet population [*Runov et al.*, 2009; *Sergeev et al.*, 2009]. In the presence of large-amplitude DFs, Maxwell tension increases dramatically. If this tension is not balanced by the thermal pressure gradient, the dipolarized flux tube accelerates inward. In terms of flux tube entropy, $S \sim p/B_z$ experiences a step-like decrease, propelling the dipolarized flux tube deeper inward and leading to acceleration of ambient plasma ahead of the front. Thus, formation of a dipolarization region seems to be an essential element in heated BBF plasma intrusion into the near-Earth plasma sheet.

[6] Observations indicate, however, that appearance of a dipolarization front does not coincide with plasma flow onset. An increase in plasma velocity, typically observed about a minute before front appearance [*Sergeev et al.*, 2009; *Runov et al.*, 2011], is due to gradual acceleration of ambient plasma ahead of it. *Zhou et al.* [2010] suggested a mechanism of ion pickup acceleration by an earthward moving DF based on a kinetic model of ion motion in the step-like increasing magnetic field. Using the MHD approach, acceleration of ambient plasma may also be explained as fast mode waves running ahead of the front.

[7] Imbalance between the Maxwell tension and the total pressure gradient produces a slingshot effect on the ambient plasma ahead of the dipolarization front. This effect has also been recognized by *Panov et al.* [2010a, 2010b], who showed that the flow bursts interact with the inner magnetosphere recoil via pressure gradient force, initiating a damped oscillatory motion in the Pi2 frequency range.

[8] In this paper, we consider in detail the force densities acting on plasma at an earthward moving dipolarization

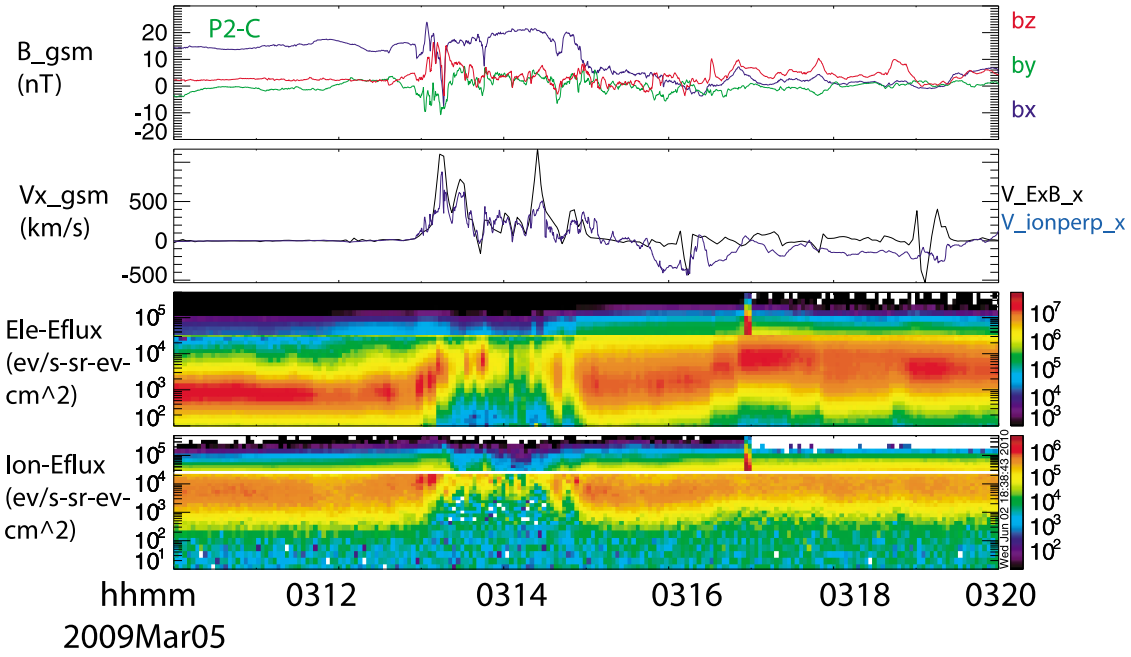

Figure 2. Field and plasma properties observed at THEMIS-C (P2). From top to bottom (GSM coordinate system): magnetic field, V_x, energy-time (ET) spectrograms for electrons, energy-time (ET) spectrograms for ions. In the first panel, magnetic field GSM components B_x, B_y, and B_z are plotted using blue, green, and red lines, respectively. The black line in the second panel represents the x component of $\mathbf{E} \times \mathbf{B}$ drift velocity, where E_x, E_y are obtained from EFI measurement and E_z is calculated assuming $\mathbf{E} \cdot \mathbf{B} = 0$ with magnetic field data from FGM measurement. The blue line in the second panel represents the x component of flow velocity calculated from ion fluxes measured by ESA and SST instruments.

front embedded into fast bulk flow in the near-Earth plasma sheet. Using the comprehensive data set from THEMIS [*Angelopoulos et al.*, 2008; *Sibeck and Angelopoulos*, 2008], we select a case with probe separation suitable for magnetic field curvature estimation and compare the estimated Maxwell tension (curvature force density) in the Earthward direction with the corresponding total pressure gradient. We seek to explain the force imbalance and consequent acceleration in the vicinity of the front. Of particular interest to us is the increase in the curvature force during magnetic field dipolarization when the field line curvature radius is actually increasing.

2. Observations and Analysis

[9] An event that occurred between 0310 and 0320 UT on 5 March 2009 is examined. Figure 1 shows THEMIS probe locations in the *XZ*, *XY*, and *YZ* GSM planes at 0314:00 UT. The three innermost probes (P3/THD, P4/THE, P5/THA) formed a closely separated cluster at around X = −10 R_E; P2/THC monitored the midtail plasma sheet at X = −18 R_E. (Data from P1/THB, which was located in the northern lobe, are not used in this paper.) We analyze data from the probes' Fluxgate Magnetometer (FGM) [*Auster et al.*, 2008], Electric Field Instrument (EFI) [*Bonnell et al.*, 2008], Electrostatic Analyzer (ESA) [*McFadden et al.*, 2008], and Solid State Telescope (SST) Instrument.

[10] Figure 2 shows P2 magnetic field and particle observations. Located in the northern half of the plasma sheet ($B_x \approx 15$ nT), P2 observed a quiet, cool plasma sheet (about 1 20 keV). Beginning at 0312:30 UT, P2 observed variations in all three magnetic field components and increases in ion and electron energy and plasma bulk velocity. During flow passage, B_x at P2 changed from 15 nT (before 0313 UT) to almost zero (after 0315 UT), which indicates that P2 was originally located in the northern half of the plasma sheet and subsequently close to the neutral sheet, presumably due to current sheet expansion. However, dipolarization appeared gradually at P2.

[11] Figure 3 gives a summary of P3(THD), P5(THA), and P4(THE) observations for the same period as shown in Figure 2. The small B_x value detected by P3 and P4 indicates that the probes were located very close to the neutral sheet. P5 was located in the southern half of the plasma sheet with a B_x level of −30 nT. A sudden jump in the B_z component, referred to as a dipolarization front, was detected by all three probes within 13 s at around 0314 UT. The front was accompanied by changes in particle energy spectrograms, similar for all three probes, indicating that the probes crossed a boundary between distinct plasma populations: cool, ambient plasma sheet and the hot plasma populating the dipolarized flux tube.

[12] Figure 4 shows the front as a clear boundary for P3 and P4. Moreover, the THEMIS pseudo-*AE* and Kyoto *AE* indices show onset signatures around the time of front arrival (not shown here).

[13] Since P3 and P4 were close to the neutral sheet where B_z component dominates, the V_x component was mostly

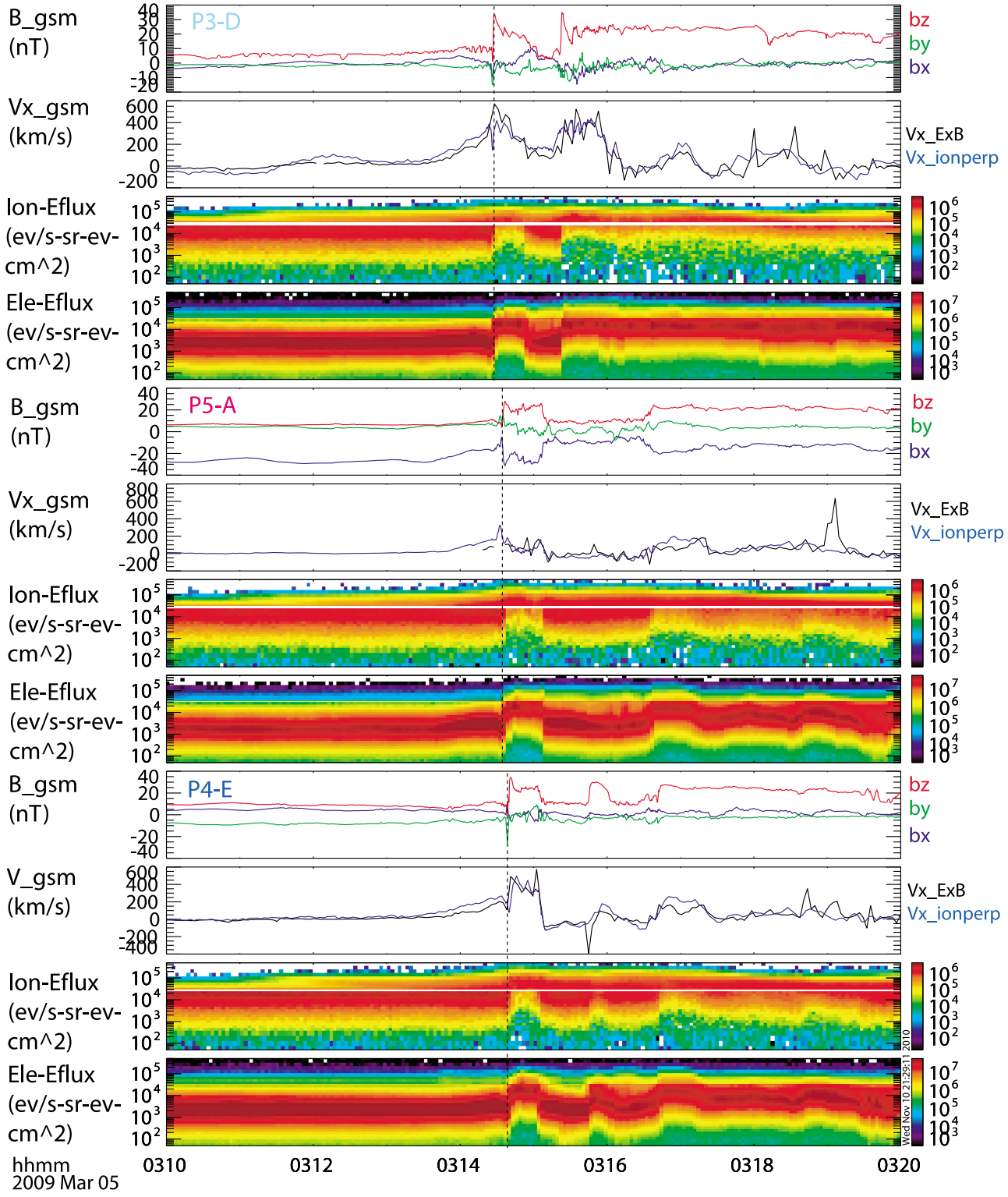

Figure 3. Overview of the field and plasma properties encountered by THEMIS-P3/P5/P4 (THD/THA/THE) around the arrival of the dipolarization front. For each probe, four panels are shown from top to bottom (GSM coordinate system): magnetic field, X component of perpendicular flow velocity (in blue), $\mathbf{E} \times \mathbf{B}$ drift velocity (in black), ion energy spectrum, electron energy spectrum.

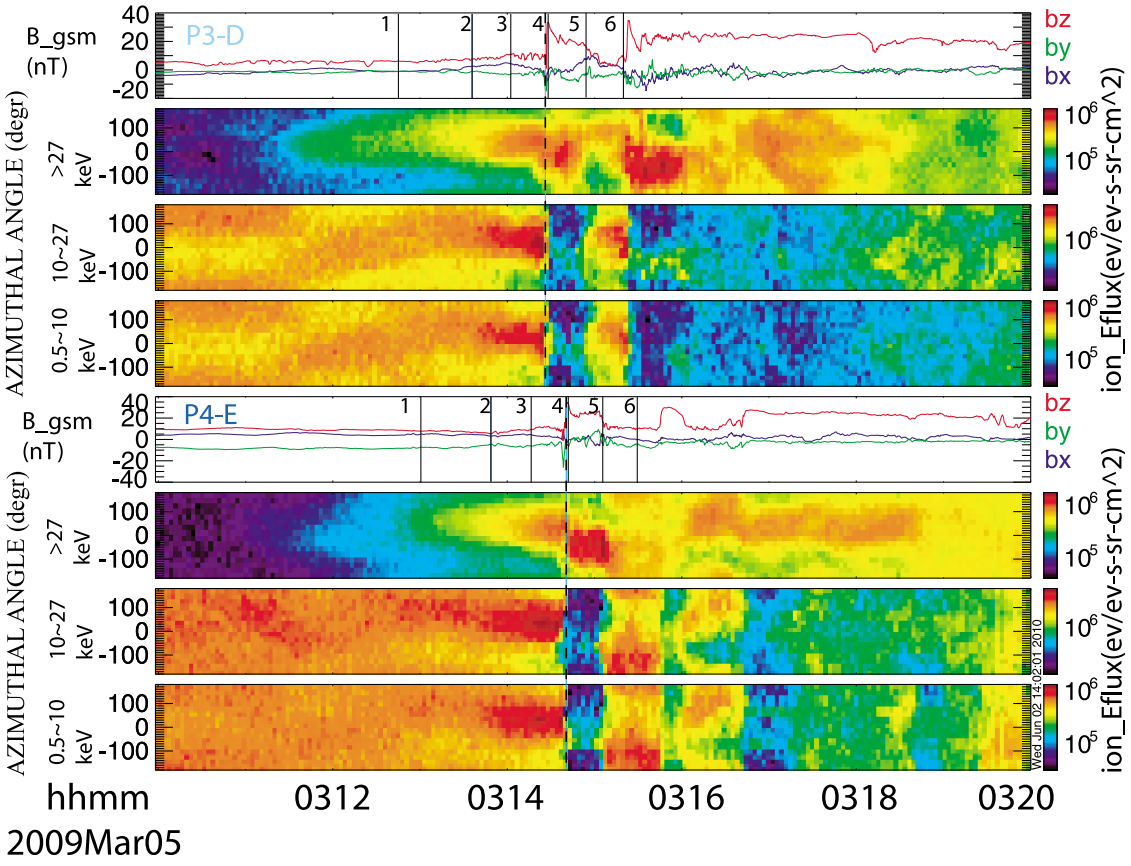

Figure 4. Dipolarization front as a boundary separating local cold plasma from hot, earthward propagating plasma. Results for P3/THD and P4/THE are shown. Below the magnetic field data, plots represent particle energy flux spectrum in azimuthal angle in three energy ranges: over 27 keV, 10 to 27 keV, and 0.5 to 10 keV. In the lower energy range, very little cold plasma is detected inside the dipolarized flux tube, whereas higher densities are detected prior to front arrival. In the higher energy range, the energetic population is only detected within 2 min of front arrival, in good correlation with the flow increase. The hot plasma detected ahead of the front is consistent with local plasma acceleration. The 1 to 6 mark six times at which our fit results are shown pictorially in Figure 5. The time shifting is clearly seen as described in the data analysis session.

perpendicular to the local magnetic field. Thus, as expected, agreement between the X components of the perpendicular ion flow velocity (blue) and $\mathbf{E} \times \mathbf{B}$ drift velocity (black) was observed ahead of the front; most of the particles are in the ESA energy range in the following energy flux spectrum plot. Furthermore, as evidenced by the ion spectra moments (not shown here), a density drop and a temperature rise were also observed by all three probes after front passage.

3. Data Analysis

[14] Timing of front arrival at P3 and P4, located at $X = -10.3$ and $X = -9.2$ R_E, respectively, reveals its earthward propagation at a velocity of 540 km/s, though the average velocity behind the front was 400 km/s. P5, located at the same X and Y as P4, detected the front and the energetic plasma population 5 s earlier than P4. This delay is consistent with assumption of an inward moving, but curved (on both XY and XZ planes) front of a flux tube with depleted entropy [*Birn et al.*, 2004; *Wolf et al.*, 2009]. This assumption is also consistent with the front normal direction shown in Table 1, evaluated using minimum variance analysis (MVA) [*Sonnerup and Scheible*, 1998]: Note that the normal direction is plotted projected on the XY and YZ GSM planes in Figure 1. However, because the front normal has a nonnegligible Y component, the 540 km/s velocity is not appropriate for further calculation. Thus in the following estimation, the average X component velocity after the front is assumed to be the earthward propagation velocity of this flow burst, approximately 400 km/s.

[15] To evaluate the force density balance at the front, we compare the curvature force density F_{curv} and the total

Table 1. Eigenvalues and Front Normal Directions of P3/P4/P5[a]

Probe	Eigenvalue $\lambda1,\lambda2,\lambda3$	Normal Direction	Location
P3-THD	146.9, 15.1, 0.17	(0.82,−0.57,−0.04)	(−10.3,1.5,−1.8) Re
P4-THE	203.6, 19.7, 0.18	(0.93,0.34,0.14)	(−9.2,2.4,−1.6) Re
P5-THA	188.9, 14.2, 0.45	(0.64,0.23,0.74)	(−9.1,2.4,−2.3) Re

[a]Normal direction is chosen as the minimum variance direction obtained by MVA method and written in X positive.

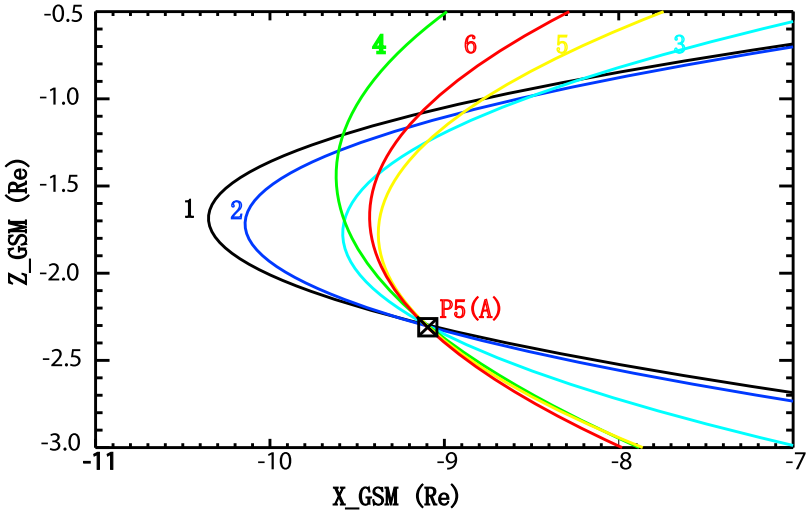

Figure 5. Field line parabolic fits for times denoted as 1 to 6 in Figure 4. Specifically, time 4 occurs right after the passage of the front structure. The field line has obviously just dipolarized. Since the field line shape is based on a fit to data from all three probes, only field lines connected to P5 are plotted here.

pressure gradient force density F_{grad}; both are derived from MHD momentum functions as represented in

$$\rho\left(\frac{\partial \mathbf{u}}{\partial t} + (\mathbf{u}\cdot\nabla)\mathbf{u}\right) = \mathbf{j}\times\mathbf{B} - \nabla P$$

$$\mathbf{j}\times\mathbf{B} = \frac{1}{\mu_0}(\nabla\times\mathbf{B})\times\mathbf{B} = -\nabla\frac{B_z^2}{2\mu_0} + (\mathbf{B}\cdot\nabla)\mathbf{B}/\mu_0$$

$$F_{\text{total}} = F_{\text{grad}} + F_{\text{curv}} = -\nabla\left(\frac{B_z^2}{2\mu_0} + P_{\text{th}}\right) + (\mathbf{B}\cdot\nabla)\mathbf{B}/\mu_0$$

[16] Since all of the three spacecraft were located close to the neutral sheet, we only evaluated the X component of the force density. As part of the $\mathbf{j}\times\mathbf{B}$ force, the curvature force vector points in the X direction earthward, at the equatorial plane. The other part of the $\mathbf{j}\times\mathbf{B}$ force, the magnetic pressure gradient, forms the total pressure gradient term ∇P_{total} together with the thermal pressure gradient. Data from P3 and P4 were used to calculate pressure gradient force density, because they were located near the equatorial plane. The total pressure gradient force density is calculated using

$$F_{\text{grad}_x} = F_{\text{grad}_x}(\text{quiet}) + \left(\frac{\delta(P_{\text{th}} + P_{\text{B}})}{\delta t}\right)/V_x$$

In this equation, V_x is a constant representing the velocity of front propagation, which is obtained by timing of the front motion. The F_{grad_x} (quiet) term is assumed to be a constant that balances the curvature force at quiet time before the front disturbance took place. The curvature force density in X direction can be obtained by two different methods. The first method (equation (1)) implies an estimation of the magnetic field curvature radius (R_{curv}):

$$F_{\text{curv}_x} = \left(\frac{B_z^2}{\mu_0}\right)/(R_{\text{curv}})_{\min} \quad (1)$$

Using multipoint measurements, the magnetic field curvature radius may be estimated by fitting the magnetic field, measured by different probes as a parabola. To evaluate R_{curv}, observations at the three innermost probes (THD/P3, THE/P4, and THA/P5) were used. As shown in Figure 3, the similarity between magnetic field variations observed by the innermost probes and their close separation suggest similarly shaped magnetic field lines at the dipolarization front. In other words, we assume the three probes have experienced exactly the same variation in field line structure, only at different locations. To account for the propagation of the BBF, we shifted the magnetic field time series in time for each individual probe so as we have three-point observations of the same field line at each relative time. This relative time series with t_0 set as the front detection time are also shown in Figure 4, where the 1 to 6 mark six relative time points. The shifting is obviously seen from Figure 4. For simplicity, we assume a 2-D parabolic field line shape expressed as $x = a(z-b)^2 + c$, where all of the parameters are time dependent. After shifting, magnetic field (B_x,B_z) and probe position (X,Z) data are linearly fitted to the function $B_x/B_z = 2a(Z-b)$. The fitting results indicate field line shape change from more stretched to more dipolarized as the DF passed the probes (shown in Figure 5). Again, 1 to 6 (the front passed at time 4) in Figure 5 mark the same relative times as Figure 4.

[17] The second method of curvature force estimation is based on the modified Harris-type model of a current sheet with a uniform normal magnetic field component. In this model, the magnetic field is $\mathbf{B} = (B_x, 0, B_z)$, where B_x depends only on the vertical coordinate z:

$$B_x = B_{\text{lobe}}\tanh\left(\frac{z-z_0}{\lambda}\right), B_z = \text{constant}$$

Here B_{lobe} is the lobe magnetic field strength, z_0 is the neutral sheet ($B_x = 0$) coordinate, and λ is the current sheet half thickness. In this model, the curvature force x component may be expressed as

$$F_{\text{curv}_x} = (B_z\cdot B_{\text{lobe}})/\mu_0\lambda \quad (2)$$

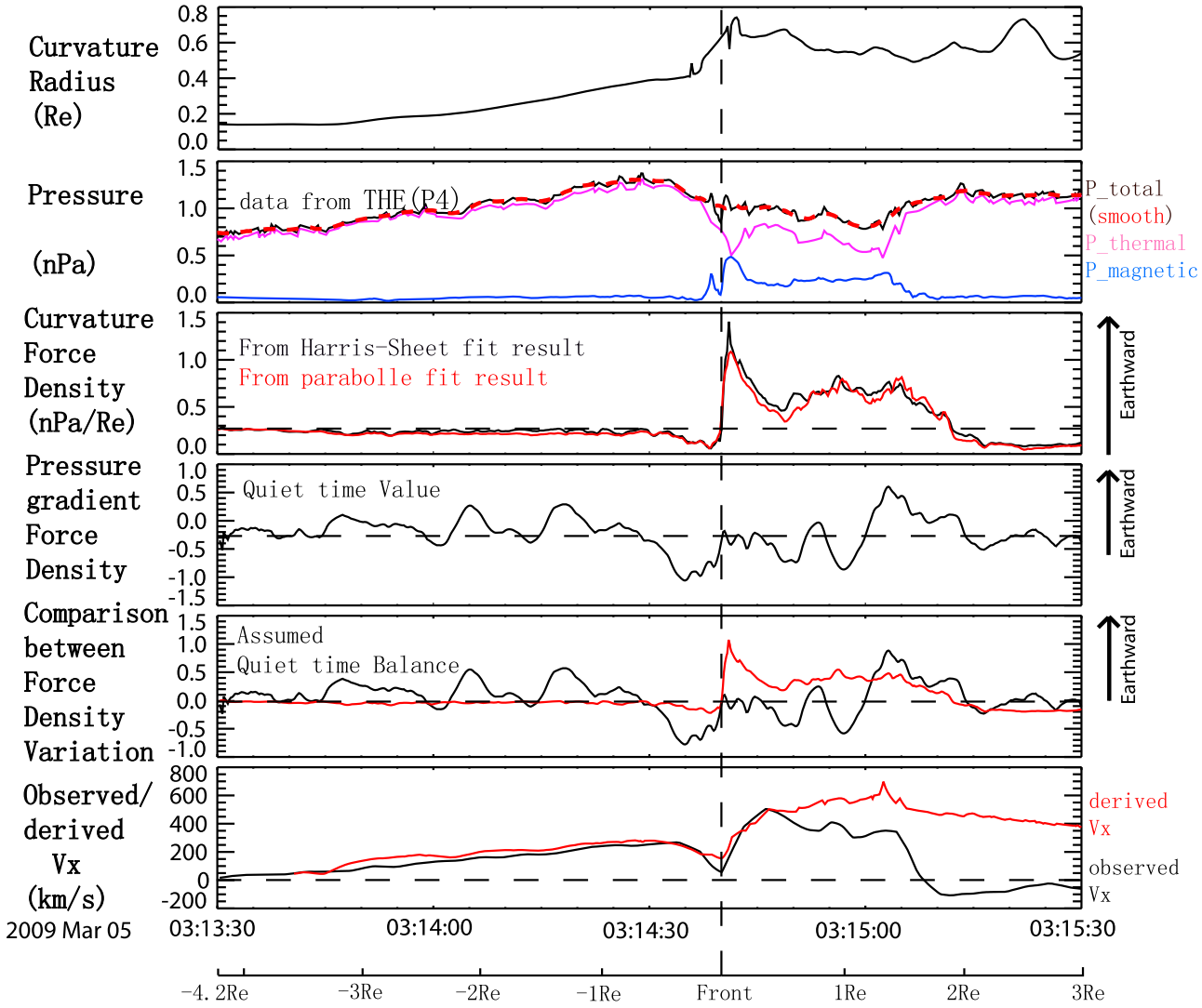

Figure 6. The first panel shows the curvature radius variance obtained from the parabola fitting. The second panel shows the pressure structure observation by P4/THE: magnetic pressure in blue, thermal pressure in magenta, and total pressure in black; the smoothed total pressure is represented by the red dashed line. The third panel shows the agreement of curvature force density estimation obtained by the two methods, and the fourth panel shows the pressure gradient force variation based on the assumed quiet time value, which is 0.28 nPa/R_E in this case. In the second, third, and fourth panels, positive/negative always shows earthward/tailward. The fifth panel shows the comparison of force density variation in the X GSM direction between curvature force density and total pressure gradient force density within the spatial structure around the DF. In the sixth panel, agreement is achieved both ahead of and immediately after the front between the observed X component velocity and that derived from the total X component force shown in the fourth panel. Ahead of the front, the increase in the pressure gradient earthward accelerates the local cold plasma. Behind the front, the larger earthward increase curvature force density overtakes the tailward increase pressure gradient force density, and hence accelerates the flux tube.

In our case, the fit to the modified Harris function may be done easily because the two probes (P4 and P5) located at approximately the same x were separated along z. With the data from P4 and P5, we can fit B_{lobe},z_0 and λ from B_x and Z, and thus obtain the curvature force density. Results from the two methods are plotted in Figure 6. In the third panel in Figure 6, curvature force density shown in the red line from parabola fitting and the black line using the Harris sheet assumption are in good agreement.

[18] By assuming a balance between curvature force F_{curv} and pressure gradient force F_{grad} at a quiet time prior to DF detection at 0314 UT when the flow was small, we evaluate only variations in these two force densities assuming they are caused by the approach of the dipolarized flux. The first panel in Figure 6 shows the pressure variation detected by THE/P4, which is similar in structure to those detected by THD/P3 and THA/P5 (because of the similarity, neither of the latter variations is shown here). Ignoring the absolute pressure

differences between different probes as due to small differences in efficiency factors, we obtain the pressure gradient force density from the temporal file of the pressure by assuming a constant propagation velocity of 400 km/s in the vicinity of the front. Only data from THE/P4 are analyzed with the equation mentioned before, and the pressure gradient force is represented in the third panel in Figure 6. The comparison between curvature force density and pressure gradient force density variations in x is shown in the fourth panel in Figure 6. The force density imbalance begins about 50 s ahead of front arrival due to a decrease in the tailward pressure gradient force density. This is consistent with the time at which the velocity starts to enhance ahead of the front in similar studies by *Runov et al.* [2011]. The consistency between force-derived velocity and observations shown in Figure 6 supports the idea that the pressure gradient accelerates the local plasma ahead of the earthward propagating front structure.

[19] Because of the increase in B_z, the earthward directed curvature force density increased ~0.6 nPa/Re on average with respect to the quiet time value after front passage. The total pressure gradient force density, directed tailward most of the time(as shown in the third panel in Figure 6), increased only 0.3 nPa/Re on average. Thus, there was a factor of 2 or greater imbalance between the Maxwell tension (F_{curv}) at the dipolarization front and the total pressure gradient, which explains the following detected acceleration of the energetic plasma inside the tube.

[20] However, over large distances, the plasma within the dipolarization flux tube decelerated slightly rather than accelerating. We show that from −18 R_E (P2) to −10 R_E in this case, which is different from our estimation of local acceleration in the vicinity of the front and thus makes the force balance issue more complicated and await for larger scale of force estimation.

4. Discussion and Conclusions

[21] We presented a THEMIS case study of an inward propagating dipolarization front embedded in a bursty bulk flow. The configuration of the THEMIS probes allowed us to detect the BBF in the plasma sheet at $X = -18$ R_E and the dipolarization front at $X = -10$ and -9 R_E sequentially. The time delay indicates earthward motion of the front at a velocity of over 500 km/s. The front normal in the vicinity of the neutral sheet was mainly in the $(XY)_{GSM}$ plane with a greater X component and a nonnegligible Y component as shown in Figure 1. It is notable that the front normal Y component was directed dawnward at $Y = 1.5$ R_E(P3) and duskward at $Y = 2.4$ R_E(P4/P5). This large difference in front normal direction within a cross-tail distance of 1 R_E indicates a front curvature radius smaller than 1 R_E on the XY plane, which may be an inherent property of flux bundles in dipolarization fronts or due to the development of interchange instability on the leading edge of the BBF [*Pritchett and Coroniti*, 2010].

[22] The main goal of our study was to evaluate the origin and effect of local pressure force balance at dipolarization fronts. Although MVA reveals the 3-D nature of the DF surface, we assume that effects of front nonplanarity do not significantly affect forces along the X direction and therefore use a 2-D geometric representation of the magnetic field lines in the force balance analysis. We evaluated the force density balance at the front by comparing the X components of the Maxwell tension F_{curv} and the total pressure gradient ($\nabla_x P_{total}$). The magnetic field curvature radius was estimated by fitting the observed magnetic field to (1) the parabolic function and (2) the modified Harris function with a uniform B_{mz}. Both methods produced similar estimates of F_{curv}, as indicated by the third panel in Figure 6.

[23] The comparison reveals dominant $\nabla_x P_{total}$ variation along X ahead of the front. Within the dipolarization front, however, the curvature forces increased dramatically, while the total pressure gradient did not change as much. Although the current sheet half thickness, λ, increased to twice the original thickness at quiet time, the increase in F_{curv} was determined by the step-like increase in B_z, which prevailed over the increase in λ. The observed imbalance between Maxwell tension and total pressure gradient at the front resulted in earthward acceleration of the dipolarized flux tube, which was separated from the ambient plasma by the front. The hot, tenuous population of the dipolarized plasma tube (BBF/bubble) therefore intruded into the near-Earth plasma sheet.

[24] Another important effect, related to the observed force density imbalance is ambient plasma acceleration ahead of the front resulting from plasma compression by the dipolarized flux tube. Analysis of P3 and P4 observations has indeed revealed an increase in the earthward total pressure gradient about 3.5 R_E ahead (earthward) of the front without significant change in the curvature force density. Decrease in the tailward pressure gradient leads to the observed earthward acceleration of ambient plasma (Figures 3 and 4). Enhancement of earthward streaming ion flux, often observed ahead of DFs, has been previously explained as ion pickup at the front [*Zhou et al.*, 2010, 2011]. Our event study shows that ambient plasma acceleration may also be explained in the MHD framework by increase in the local pressure gradient force density. Distribution function analysis can distinguish between the two mechanisms, by revealing whether a second (picked up) population is superimposed on preexisting plasma, or a single accelerated component is responsible for the flow velocity increase.

[25] Our case study suggests that flow bursts accompanied by a large-amplitude dipolarization front will penetrate deeper into the dipole-dominated, near-Earth plasma sheet due to the predominance of the curvature force density. This force results primarily from the magnetic field increase that builds up to compensate the density depletion within the dipolarized flow burst. Further statistical analysis would be needed to determine how common these results are. However, we note that the characteristics of the flow bursts surrounding a dipolarization front, the pressure increase ahead of it and the sudden increase in B_z are common to all events examined, and based on this we anticipate this mechanism to be common rather than fortuitous.

[26] **Acknowledgments.** We acknowledge NASA contracts NAS5-02099 and NNX08AD85G, the German Ministry for Economy and Technology, and the German Center for Aviation and Space (DLR), contract 50 OC 0302. We thank P. L. Pritchett and L. Lyons for discussions and B. Kerr, P. Cruce, M. Feuerstein, and J. Hohl for help with software and editing. *AE* index data were provided by the World Data Center for Geomagnetism in Kyoto. We acknowledge C. T. Russell, S. B. Mende, I. R. Mann, and

M. Connors, who provided geomagnetic data to calculate the THEMIS pseudo-*AE* index.

[27] Robert Lysak thanks the reviewers for their assistance in evaluating this paper.

References

Angelopoulos, V., et al. (1994), Statistical characteristics of bursty bulk flow events, *J. Geophys. Res.*, *99*, 21,257–21,280, doi:10.1029/94JA01263.

Angelopoulos, V., et al. (2008), First results from the THEMIS mission, *Space Sci. Rev.*, *141*, 453–476, doi:10.1007/s11214-008-9378-4.

Auster, H. U., et al. (2008), The THEMIS fluxgate magnetometer, *Space Sci. Rev.*, *141*, 235–264, doi:10.1007/s11214-008-9365-9.

Baumjohann, W., M. Hesse, S. Kokubun, T. Mukai, T. Nagai, and A. A. Petrukovich (1999), Substorm dipolarization and recovery, *J. Geophys. Res.*, *104*, 24,995–25,000, doi:10.1029/1999JA900282.

Birn, J., J. Raeder, Y. Wang, R. Wolf, and M. Hesse (2004), On the propagation of bubbles in the geomagnetic tail, *Ann. Geophys.*, *22*, 1773–1786, doi:10.5194/angeo-22-1773-2004.

Bonnell, J. W., F. S. Mozer, G. T. Delory, A. J. Hull, R. E. Ergun, C. M. Cully, V. Angelopoulos, and P. R. Harvey (2008), The Electric Field Instrument (EFI) for THEMIS, *Space Sci. Res.*, *141*, 303–341, doi:10.1007/s11214-008-9469-2.

Dubyagin, S., V. Sergeev, S. Apatenkov, V. Angelopoulos, R. Nakamura, J. McFadden, D. Larson, and J. Bonnell (2010), Pressure and entropy changes in the flow-braking region during magnetic field dipolarization, *J. Geophys. Res.*, *115*, A10225, doi:10.1029/2010JA015625.

McFadden, J. P., C. W. Carlson, D. Larson, J. Bonnell, F. Mozer, V. Angelopoulos, K.-H. Glassmeier, and U. Auster (2008), THEMIS ESA first science results and performance issues, *Space Sci. Rev.*, *141*, 477–508, doi:10.1007/s11214-008-9433-1.

Ohtani, S., M. A. Shay, and T. Mukai (2004), Temporal structure of the fast convective flow in the plasma sheet: Comparison between observations and two-fluid simulations, *J. Geophys. Res.*, *109*, A03210, doi:10.1029/2003JA010002.

Panov, E. V., et al. (2010a), Plasma sheet thickness during a bursty bulk flow reversal, *J. Geophys. Res.*, *115*, A05213, doi:10.1029/2009JA014743.

Panov, E. V., et al. (2010b), Multiple overshoot and rebound of a bursty bulk flow, *Geophys. Res. Lett.*, *37*, L08103, doi:10.1029/2009GL041971.

Pritchett, P. L., and F. V. Coroniti (2010), A kinetic ballooning/interchange instability in the magnetotail, *J. Geophys. Res.*, *115*, A06301, doi:10.1029/2009JA014752.

Runov, A., V. Angelopoulos, M. I. Sitnov, V. A. Sergeev, J. Bonnell, J. P. McFadden, D. Larson, K.-H. Glassmeier, and U. Auster (2009), THEMIS observations of an earthward-propagating dipolarization front, *Geophys. Res. Lett.*, *36*, L14106, doi:10.1029/2009GL038980.

Runov, A., et al. (2011), Dipolarization fronts in the magnetotail plasma sheet, *Planet. Space Sci.*, *59*, 517–525, doi:10.1016/j.pss.2010.06.006.

Sergeev, V. A., V. Angelopoulos, J. T. Gosling, C. A. Cattell, and C. T. Russell (1996), Detection of localized, plasma-depleted flux tubes or bubbles in the midtail plasma sheet, *J. Geophys. Res.*, *101*, 10,817–10,826, doi:10.1029/96JA00460.

Sergeev, V. A., K. Liou, P. T. Newell, S.-I. Ohtani, M. R. Hairston, and F. Rich (2004), Auroral streamers: Characteristics of associated precipitation, convection and field-aligned currents, *Ann. Geophys.*, *22*, 537–548, doi:10.5194/angeo-22-537-2004.

Sergeev, V., V. Angelopoulos, S. Apatenkov, J. Bonnell, R. Ergun, R. Nakamura, J. McFadden, D. Larson, and A. Runov (2009), Kinetic structure of the sharp injection/dipolarization front in the flow-braking region, *Geophys. Res. Lett.*, *36*, L21105,doi:10.1029/2009GL040658.

Shiokawa, K., et al. (1998), High-speed ion flow, substorm current wedge, and multiple Pi 2 pulsations, *J. Geophys. Res.*, *103*, 4491–4507, doi:10.1029/97JA01680.

Sibeck, D. G., and V. Angelopoulos (2008), THEMIS science objectives and mission phases, *Space Sci. Rev.*, *141*, 35–59, doi:10.1007/s11214-008-9393-5.

Sitnov, M. I., M. Swisdak, and A. V. Divin (2009), Dipolarization fronts as a signature of transient reconnection in the magnetotail, *J. Geophys. Res.*, *114*, A04202, doi:10.1029/2008JA013980.

Sonnerup, B. U. Ö., and M. Scheible (1998), Minimum and maximum variance analysis, in *Analysis Methods for Multi-Spacecraft Data*, *ISSI Sci. Rep. Ser.*, vol. 1. edited by Götz Paschmann and Patrick Daly, pp. 185–220, Eur. Space Agency, Noordwijk, Netherlands.

Wolf, R. A., V. Kumar, F. R. Toffoletto, G. M. Erickson, A. M. Savoie, C. X. Chen, and C. L. Lemon (2006), Estimating local plasma sheet pv5/3 from single spacecraft observations, *J. Geophys. Res.*, *111*, A12218, doi:10.1029/2006JA012010.

Wolf, R. A., Y. Wan, X. Xing, J.-C. Zhang, and S. Sazykin (2009), Entropy and plasma sheet transport, *J. Geophys. Res.*, *114*, A00D05, doi:10.1029/2009JA014044.

Zhou, X.-Z., V. Angelopoulos, V. A. Sergeev, and A. Runov (2010), Accelerated ions ahead of earthward propagating dipolarization fronts, *J. Geophys. Res.*, *115*, A00I03, doi:10.1029/2010JA015481.

Zhou, X.-Z., V. Angelopoulos, V. A. Sergeev, and A. Runov (2011), On the nature of precursor flows upstream of advancing dipolarization fronts, *J. Geophys. Res.*, *116*, A03222, doi:10.1029/2010JA016165.

V. Angelopoulos, S. Li, A. Runov, and X.-Z. Zhou, Department of Earth and Space Science, University of California, Geology Bldg. 3697, Los Angeles, CA 90024, USA. (susanlss@ucla.edu)

U. Auster, Institut für Geophysik und Extraterrestrische Physik, Technische Universität, Mendelssohnstrasse 3, D-38106 Braunschweiger, Germany.

J. Bonnell, D. Larson, and J. McFadden, Space Sciences Laboratory, University of California, 7 Gauss Way, Berkeley, CA 94720-7450, USA.